

Published in final edited form as:

Nat Catal. 2018 January ; 1(1): 55–62. doi:10.1038/s41929-017-0001-5.

## Selective aerobic oxidation reactions using a combination of photocatalytic water oxidation and enzymatic oxyfunctionalisations

Wuyuan Zhang<sup>[a]</sup>, Elena Fernández-Fueyo<sup>[a]</sup>, Yan Ni<sup>[a]</sup>, Morten van Schie<sup>[a]</sup>, Jenö Gacs<sup>[a]</sup>, Rokus Renirie<sup>[b]</sup>, Ron Wever<sup>[b]</sup>, Francesco G. Mutti<sup>[b]</sup>, Dörte Rother<sup>[c]</sup>, Miguel Alcalde<sup>[d]</sup>, and Frank Hollmann<sup>[a]\*</sup>

<sup>[a]</sup>Department of Biotechnology, Delft University of Technology, Van der Maasweg 9, 2629HZ Delft, The Netherlands <sup>[b]</sup>Van't Hoff Institute for Molecular Sciences (HIMS), Faculty of Science, University of Amsterdam, Science Park 904, 1098 XH Amsterdam, The Netherlands <sup>[c]</sup>Institute of Bio- and Geosciences, IBG-1: Biotechnology, Forschungszentrum Jülich GmbH, 52425 Jülich, Germany <sup>[d]</sup>Department of Biocatalysis, Institute of Catalysis, CSIC, 28049 Madrid, Spain

### Abstract

Peroxygenases offer attractive means to address challenges in selective oxyfunctionalisation chemistry. Despite their attractiveness, the application of peroxygenases in synthetic chemistry remains challenging due to their facile inactivation by the stoichiometric oxidant (H<sub>2</sub>O<sub>2</sub>). Often atom inefficient peroxide generation systems are required, which show little potential for large scale implementation. Here we show that visible light-driven, catalytic water oxidation can be used for *in situ* generation of H<sub>2</sub>O<sub>2</sub> from water, rendering the peroxygenase catalytically active. In this way the stereoselective oxyfunctionalisation of hydrocarbons can be achieved by simply using the catalytic system, water and visible light.

### Introduction

Selective oxyfunctionalisation of carbon-hydrogen bonds still represents a dream reaction in organic synthesis. 1, 2, 3 Particularly, balancing reactivity of the oxygen-transfer reagent with selectivity is largely unsolved for (in)organic catalysts while it is an inherent feature of many oxidative enzyme such as heme-dependent monooxygenases and peroxygenases. The

---

Users may view, print, copy, and download text and data-mine the content in such documents, for the purposes of academic research, subject always to the full Conditions of use:[http://www.nature.com/authors/editorial\\_policies/license.html#terms](http://www.nature.com/authors/editorial_policies/license.html#terms)

\* f.hollmann@tudelft.nl.

#### Data Availability

All data is available from the authors upon reasonable request.

#### Author contributions

WZ, EFF, YN, MvS and JG performed the experimental work and analysed the results; RR, RW, FGM, DR and MA provided biocatalysts and participated in the planning and analysis of the experiments; WZ and FH conceived and designed the experiments. All authors co-wrote the manuscript.

#### Competing Financial Interest

The authors declare no competing financial interests.

relevance of peroxygenases (UPO for *unspecific* peroxygenase, E.C. 1.11.2.1) for selective oxyfunctionalisation reactions in preparative organic synthesis is increasing rapidly.<sup>4</sup> Especially the ‘novel’ peroxygenases from *Agrocybe aegerita* (AaeUPO),<sup>5</sup> *Marasmius rotula* (MroUPO)<sup>6</sup> or *Coprinopsis cinerea* (CcuUPO)<sup>7</sup> excel in terms of substrate scope and specific activity over the well-known chloroperoxidase from *Caldariomyces fumago* (CfuUPO),<sup>8</sup> P450 monooxygenases and chemical counterparts. The very high turnover numbers (TONs) reported so far give reason to expect truly preparative-scale applications of these very promising biocatalysts. Additionally, crystal structures of AaeUPO<sup>9</sup> as well as directed evolution protocols<sup>10</sup> together with efficient recombinant expression systems have been established in the past few years. Hence, current gaps in substrate scope, stability and/or selectivity will be closed.<sup>1, 11, 12, 13</sup>

In contrast to P450 monooxygenases, peroxygenases do not rely on complicated and susceptible electron transport chains delivering reducing equivalents to the heme active site needed for reductive activation of molecular oxygen and therefore are not subject to the *Oxygen Dilemma*.<sup>14</sup> Rather, peroxygenases utilise H<sub>2</sub>O<sub>2</sub> directly to regenerate the catalytically active oxoferyl heme species. At the same time, however, peroxygenases suffer (like all heme-dependent enzymes) from a pronounced instability against H<sub>2</sub>O<sub>2</sub> making controlled *in situ* provision with H<sub>2</sub>O<sub>2</sub> inevitable. Today, the well-known glucose/glucose oxidase system to generate H<sub>2</sub>O<sub>2</sub> from O<sub>2</sub> prevails on lab-scale; but shows little potential for larger, preparative applications due to its poor atom-efficiency.<sup>15</sup> More efficient electron donors such as small alcohols or electrochemical sources have recently been proposed.<sup>16, 17</sup>

Ideally, water could serve as co-substrate and electron donor for *in situ* generation of H<sub>2</sub>O<sub>2</sub>. Peroxygenase reactions are generally conducted in aqueous media (c(H<sub>2</sub>O) = 55 mol L<sup>-1</sup>) and the sole by-product of the water oxidation reaction is molecular oxygen. A broad variety of heterogeneous water oxidation catalysts (WOCs) have been reported in recent years that could be used for the partial oxidation of water to hydrogen peroxide.<sup>18, 19</sup> The thermodynamic driving force for this reaction is derived from (visible) light. Mostly, this approach is evaluated with respect to catalytic water splitting into H<sub>2</sub> and O<sub>2</sub>. However, under aerobic conditions, electrons liberated from water can also be transferred to O<sub>2</sub> yielding H<sub>2</sub>O<sub>2</sub>. Also incomplete oxidation of water to H<sub>2</sub>O<sub>2</sub> can be conceived.

This motivated us to evaluate photochemical water oxidation yielding H<sub>2</sub>O<sub>2</sub> to promote peroxygenase-catalysed, selective oxyfunctionalisation reactions (Figure 1). In this contribution we demonstrate the general feasibility of this approach together with a characterisation of the crucial parameters determining activity and robustness of the reaction scheme. The selective, photoenzymatic oxyfunctionalisation of a range of hydrocarbons is demonstrated. Also the embedding of this reaction scheme into more extended cascades producing value-added chiral alcohols and amines is demonstrated.

## Results

### Proof-of-concept experiments

As model enzyme for our studies we chose the UPO from *Agrocybe aegerita*, which was recombinantly expressed in *Pichia pastoris* (rAaeUPO) following a previously reported

protocol.<sup>20</sup> The enzyme was purified to near homogeneity by a single anion exchange chromatography step (Supplementary Figures 5 and 6). The enzyme preparation used herein exhibited a Reinheitszahl (Rz:  $A_{420}/A_{280}$ ) value of 1.6. As model reaction we chose the stereoselective hydroxylation of ethyl benzene to (*R*)-1-phenyl ethanol (Figure 2). Visible-light active Au-loaded TiO<sub>2</sub> was used as photocatalysts for the proof-of-concept experiments.<sup>21</sup>

Under arbitrarily chosen reaction conditions (Figure 2) we were pleased to observe significant accumulation of (*R*)-1-phenyl ethanol. Control reactions in the absence of the Au-TiO<sub>2</sub> photocatalyst or in the darkness yielded no product formation. In the absence of either the enzyme or using thermally inactivated enzyme resulted in a slow accumulation of racemic 1-phenyl ethanol (less than 0.14 mM within 24 h) and approximately the same concentrations of acetophenone. This minor background oxidation activity of the photocatalyst also explains the slightly decreased optical purity of the (*R*)-1-phenyl ethanol obtained from the photobiocatalytic oxidation reactions (90% ee) as compared to traditional reaction schemes for the provision of rAaeUPO with H<sub>2</sub>O<sub>2</sub> (> 97% ee).<sup>22</sup>

Particular attention was paid to the nature of the electron donor for this reaction as in principle also other reaction components may be susceptible to TiO<sub>2</sub> oxidation and thereby serve as sacrificial electron donor for the reduction of O<sub>2</sub>. For this, the enzyme preparation contained phosphate only as buffer component to exclude possible contributions of other sacrificial electron donors to H<sub>2</sub>O<sub>2</sub> generation. Also experiments using immobilised enzymes were conducted to exclude rAaeUPO oxidation to promote H<sub>2</sub>O<sub>2</sub> generation. To further support the assumed water oxidation-based mechanism, we performed a range of experiments using <sup>18</sup>O labelled water as reaction mixture. The occurrence of <sup>18</sup>O-labelled (*R*)-1-phenylethanol (Supplementary Figure 10) substantiates the proposed mechanism. Performing this experiment in the presence of ambient air (predominantly consisting of <sup>16</sup>O<sub>2</sub>) resulted in a minor incorporation of <sup>18</sup>O into the product, which predominantly contained <sup>16</sup>O. Using deaerated reaction mixtures (wherein only water oxidation can account for O<sub>2</sub>) the <sup>18</sup>O-labelled product dominated. These findings strongly support the suggested TiO<sub>2</sub>-mediated oxidation of H<sub>2</sub>O to O<sub>2</sub> coupled to TiO<sub>2</sub>-catalysed reduction of O<sub>2</sub> to H<sub>2</sub>O<sub>2</sub> finally being used by rAaeUPO for specific incorporation into ethyl benzene. Also a contribution of H<sub>2</sub>O<sub>2</sub> originating from direct two-electron water oxidation is possible.<sup>23</sup> In any case, the above-mentioned results make us confident that water served indeed as sole source of reducing equivalents to promote the selective rAaeUPO-catalysed oxyfunctionalisation reactions.

### Characterisation of the photoenzymatic oxyfunctionalisation reaction

Next, we advanced to characterise the reaction system in more detail, particularly investigating the effect of varying catalyst concentrations on the reaction system. It is worth mentioning here that, though the product concentrations shown in Figure 2 may appear low but significantly surpass the concentrations of H<sub>2</sub>O<sub>2</sub> obtained from water oxidation reported so far for Au-TiO<sub>2</sub> and other WOCs.<sup>19, 24</sup> We attribute this to a H<sub>2</sub>O<sub>2</sub>-oxidation activity of the illuminated WOCs (Supplementary Figure 11) eventually leading to a low steady-state concentration of H<sub>2</sub>O<sub>2</sub>.<sup>25</sup> At first sight, this may appear as a limitation for the current

system, but it also enables us to maintain low, constant *in situ* concentrations of H<sub>2</sub>O<sub>2</sub> as required for efficient and robust peroxygenase catalysis.

Interestingly, the concentration of the WOC had only a minor influence on the initial rate of the reaction (Figure 2 a). We attribute this to WOC-concentration-independent *in situ* H<sub>2</sub>O<sub>2</sub> concentrations, most probably due to the simultaneous water- and H<sub>2</sub>O<sub>2</sub>-oxidation activity of the WOCs mentioned above. The WOC concentration, however, had a very significant influence on the robustness of the overall reaction. In general, no more product accumulation was observable after approx. 6 h. Varying the Au content (0.6-1.8 wt%) and particle size (2.8-7.9 nm) on the TiO<sub>2</sub> surface hardly influenced the time course of the photobiocatalytic hydroxylation reaction with the exception of plain TiO<sub>2</sub>, here the overall rate was approximately half of the rates obtained with Au-TiO<sub>2</sub> (Supplementary Figure 12).

In contrast, the enzyme concentration directly influenced the overall reaction rate (Figure 2 B) and a linear dependency of the initial (*R*)-1-phenyl ethanol accumulation on the concentration of rAaeUPO applied was observed. However, again, the reactions ceased after 6-7 h.

Apparently, the robustness of the overall reaction (as judged from the accumulation of (*R*)-1-phenyl ethanol) correlated with the ratio of photo- and bio-catalyst. We hypothesised that rAaeUPO may be inactivated by the Au-TiO<sub>2</sub>-WOC. It should be mentioned here, that in the experiments reported so far, only TiO<sub>2</sub> mostly composed of anatase phase (91.1%) had been used as WOC. Given the rather hydrophilic surface of anatase TiO<sub>2</sub>, adsorption of the glycoprotein rAaeUPO appears likely. Therefore, we performed a range of control experiments to shed light on the inactivation of the biocatalyst: incubation of the enzyme with the photocatalyst in the darkness resulted in a minor reduction of its catalytic activity as compared to the same experiment in the presence of light (Figure 3). Therefore, we conclude that not the adsorption *per se* leads to inactivation of the catalyst.

We hypothesised that reactive oxygen species (ROS) generated at the surface of the water oxidation catalyst<sup>26</sup> may account for this observation via oxidative inactivation of the enzyme. In fact, using the spin trap technique in electron paramagnetic resonance spectroscopy, significant amounts of mainly hydroxyl (HO•) radicals ( $a_H = 1.495$  mT;  $g = 2.0050$ ) could be detected in illuminated anatase Au-TiO<sub>2</sub> samples (Figure 4 a).<sup>26</sup> These hydroxyl radicals may originate from water oxidation, from the reaction of superoxide (•O<sub>2</sub><sup>-</sup>, from O<sub>2</sub> reduction) or other steps in the complex redox chemistry of ROS.<sup>27</sup> Though more detailed mechanistic studies will be necessary to fully understand this inactivation mechanism, we hypothesise a major role of the hydroxyl radical over the superoxide radical. First, addition of superoxide dismutase did not improve the robustness of the overall reaction. Second, •O<sub>2</sub><sup>-</sup> should react with native peroxygenase leading to the formation of the so-called Compound III of the catalytic cycle, for which we have not found any spectroscopic evidence (no characteristic absorption peak at 625 nm, Supplementary Figure 14).<sup>28</sup>

## Overcoming robustness issues through separation

Given the rather short half-life time of hydroxyl radicals (approx.  $10^{-9}$  s in aqueous media) we envisioned that simple spatial separation of the WOC (at which's surface the HO• radicals are being formed) and the biocatalyst may circumvent this limitation. Therefore, we evaluated (1) spatial separation of anatase Au-TiO<sub>2</sub> from rAaeUPO using immobilised enzymes and (2) avoiding rAaeUPO adsorption to the WOC surface by using hydrophobic surfaces.

To achieve physical separation of the WOC and rAaeUPO, we covalently immobilised the latter to a poly(methyl methacrylate) resin activated by glutardialdehyde. Covalent linkage to the spacer unit occurred through imine formation with surface-exposed lysine residues (Supplementary Figure 7). To test the second option, i.e. avoidance of enzyme adsorption by less hydrophilic WOC surfaces, rutile Au-TiO<sub>2</sub> was evaluated. Rutile exhibits a far more hydrophobic surface as compared to the previously used anatase catalyst. This is corroborated also by the lack of the characteristic IR-absorptions of surface-bound H<sub>2</sub>O and Ti-OH (even after Au-doping treatment) at 3422 and 1632 cm<sup>-1</sup>, respectively (Supplementary Figure 13). This leads to the assumption that the heavily glycosylated rAaeUPO may be less prone to adsorption to rutile than to anatase surfaces. Hence, while the photoelectrochemical properties (i.e. the redox potential and energy levels of conducting- and valence band)<sup>30</sup> of both crystal phases are comparable, rutile should be preferable due to its expected lower adsorption tendency for proteins. Indeed, rAaeUPO adsorbed approximately 10 times less to rutile as compared to anatase catalyst (Supplementary Figures 15 and 16). Furthermore, this effect does not appear to be limited to glycoproteins such as rAaeUPO as also a bacterial enzyme (the old yellow enzyme homologue from *Bacillus subtilis*, YqjM)<sup>31</sup> showed a similar adsorption behaviour as rAaeUPO (Supplementary Figure 17). Overall, both strategies appeared to be suitable to minimise oxidative inactivation of rAaeUPO at the photocatalyst surface and therefore should lead to more robust photobiocatalytic hydroxylation reactions. Figure 5 compares the time courses of these catalytic systems.

In both cases steady product accumulation was observed for at least 120 h thereby representing a more than 20-fold increase of the robustness as compared to the starting conditions (Figure 5 ▲). Consequently, also the turnover number of the enzyme increased from approx. 2000 using dissolved enzyme and anatase-Au-TiO<sub>2</sub> to more than 16000 or 21000 using immobilised rAaeUPO (Figure 5 ◆) or rutile-Au-TiO<sub>2</sub> (Figure 5 ■), respectively. The latter system also provided (*R*)-1-phenyl ethanol in much higher optical purity (>98% ee) as compared to the starting conditions. The reaction using immobilised rAaeUPO was considerably slower than the reaction using free rAaeUPO and rutile-Au-TiO<sub>2</sub>. This may, at least to some extent, be attributed to diffusion limitations originating from the double heterogeneous character of the catalysts. Also partial loss of enzyme activity as a consequence of the immobilisation may contribute to this.<sup>32</sup> Systematic immobilisation studies with rAaeUPO are currently ongoing to clarify this.

The average turnover frequency of rAaeUPO of 2.9 min<sup>-1</sup> (average over 4 days) indicates that there is room for improving the efficiency of this reaction system. Indeed, increasing the rutile-Au-TiO<sub>2</sub> concentration linearly increased the initial rate of the overall reaction

(Supplementary Figure 18). Surprisingly, an EPR investigation of the rutile-Au-TiO<sub>2</sub> catalysed water oxidation (Figure 4 b) revealed that this catalyst generates significantly higher amounts of HO• radicals than anatase-Au-TiO<sub>2</sub>. In fact, as already stated, a higher amount of superoxide may be formed by rutile Au-TiO<sub>2</sub>. At first sight this is in contrast to the higher compatibility of rutile-Au-TiO<sub>2</sub> with the enzymes investigated. It may, however, be rationalised by the poor adsorption tendency of proteins to the rutile-TiO<sub>2</sub> surface and the very short half life time of the hydroxyl radical resulting in very short diffusion distances.<sup>33</sup>

### Substrate scope of the photoenzymatic reaction

Encouraged by these promising results, we further explored the product scope of the photoenzymatic hydroxylation reaction using dissolved *rAaeUPO* and rutile-Au-TiO<sub>2</sub>. As shown in Table 1, a broad range of aliphatic and aromatic compounds was converted into the corresponding alcohols. The enantioselectivities and relative activities corresponded to the values reported previously indicating that the natural reactivity and selectivity of the enzyme were not impaired.<sup>34, 35</sup> Similar results were also observed in the system utilising anatase-Au-TiO<sub>2</sub> and immobilised enzyme (Supplementary Table 2). Also semipreparative-scale reactions proved to be feasible with this setup (Supplementary Figures 28-30). Hence, approx. 110 mg of highly enantioenriched (ee = 97.4%, 31% isolated yield) (*R*)-1-phenyl ethanol was produced.

The regioselectivity of all reactions was very high except for entry 7 where ω-2 and ω-3 hydroxylation products were observed. This observation is in line with previous reports on *rAaeUPO*-selectivity towards linear alkanes.<sup>36</sup>

### Cascade reactions

Generally, the only by-product observed was the ‘overoxidation’ product, i.e. the corresponding ketone. We suspected WOC-catalysed further oxidation of the primary *rAaeUPO*-product ((*R*)-1-phenyl ethanol) to account for this. Indeed, the concentration of acetophenone linearly increased with increasing concentrations of Au-TiO<sub>2</sub> (Supplementary Table 3). This dual activity of the photocatalyst (water- and alcohol oxidation) motivated us to evaluate more elaborate photoenzymatic cascades to extend the product scope beyond (chiral) alcohols. In particular, we coupled the photoenzymatic oxidation of toluene to benzaldehyde to an enzymatic benzoin condensation using the benzaldehyde lyase from *Pseudomonas fluorescens* (*PfBAL*) (Figure 6 A).<sup>37, 38</sup> Also, acetophenone, formed by the photoenzymatic oxyfunctionalisation of ethyl benzene was submitted to a reductive amination using the ω-transaminases from *Aspergillus terreus* (*R*-selective, *At*-ω-TA) and *Bacillus megaterium* (*S*-selective, *Bm*-ω-TA) (Figure 6 B).<sup>39, 40</sup> Both cascades were performed in a one-pot-two-step fashion, i.e. the photoenzymatic oxidation to the corresponding aldehyde or ketone was performed first, followed by addition of the biocatalysts needed for the second transformation (Supplementary Figures 31-35). Recently, Flitsch and coworkers reported a similar transformation (ethyl benzene to enantiomerically pure (*R*)- or (*S*)-1-phenyl ethyl amine) attaining very similar product titers.<sup>41</sup> It is worth mentioning that also a one-pot-one-step procedure was possible in case of cascade B, albeit at somewhat lower product yields (0.7 mM, 37 % ee and 0.5 mM, 99 % ee for (*R*)- and (*S*)-1-phenyl ethyl amine, respectively).

These results demonstrate that the proposed photoenzymatic cascades enable synthesis of a broader range of value-added products (chiral alcohols, amines and acyloins) from simple starting materials. While these reactions undoubtedly still need further improvement to reach preparative feasibility, they nevertheless demonstrate the principal feasibility of the envisioned photoenzymatic cascade reactions.

The proposed *in situ* H<sub>2</sub>O<sub>2</sub> generation system can also be applied to other peroxidases such as the V-dependent haloperoxidase from *Curvularia inaequalis* (CVCPO).<sup>42, 43</sup> Gratifyingly, the CVCPO-catalysed halogenation of thymol proceeded smoothly yielding 2- and 4-bromothymol with more than 70 % conversion (Figure 7). The product distribution was comparable to previous haloperoxidase-catalysed halogenation reactions.<sup>44, 45</sup> In the absence of either CVCPO, rutile-Au-TiO<sub>2</sub> or light, no conversion of thymol was observed. It is also worth mentioning that rutile-Au-TiO<sub>2</sub> with this enzyme gave better results than anatase-Au-TiO<sub>2</sub> under otherwise identical conditions.

### Beyond TiO<sub>2</sub>-based WOCs

So far, we have focussed on TiO<sub>2</sub>-based photocatalysts. Photocatalysis, however, is an extremely dynamic area of research and novel, potentially useful, WOCs are reported on an almost weekly basis. Therefore, we finally evaluated the scope of different WOCs for the *in situ* generation of H<sub>2</sub>O<sub>2</sub> to promote peroxygenase-catalysed hydroxylation reactions. Amongst them visible light-active Au-BiVO<sub>4</sub><sup>19</sup> and g-C<sub>3</sub>N<sub>4</sub><sup>46</sup> showed some promising characteristics (Supplementary Figure 36). The product formation with Au-BiVO<sub>4</sub> as photocatalyst was rather modest. g-C<sub>3</sub>N<sub>4</sub> exhibited a higher product formation rate together with a pronounced ‘overoxidation activity’ (approx. 10 times higher than Au-TiO<sub>2</sub> under comparable conditions).<sup>47</sup> Therefore, the latter catalyst may be particularly suitable for further photobiocatalytic cascades.

Finally, recently described carbon nano dot (CND) photocatalysts caught our attention as easy-to-prepare and biocompatible photocatalysts.<sup>48, 49, 50</sup> As CND-mediated reduction of molecular oxygen to H<sub>2</sub>O<sub>2</sub> is impaired<sup>48</sup> we used riboflavin monophosphate (flavin mononucleotide, FMN) as co-catalyst for the generation of H<sub>2</sub>O<sub>2</sub> (Figure 8). Visible light illumination of a mixture of CND and FMN in deaerated phosphate buffer resulted in fast and complete reduction of FMN as judged by the decrease of the characteristic absorption band of FMN<sup>Ox</sup> at 450 nm (Figure 8 b). Exposure to ambient atmosphere resulted in complete restoration of this absorbance indicating aerobic reoxidation of FMN<sup>Red</sup> yielding H<sub>2</sub>O<sub>2</sub>.

Next, we tested the photocatalytic reduction of FMN and its aerobic, H<sub>2</sub>O<sub>2</sub>-forming reoxidation to promote rAaeUPO-catalysed hydroxylation. Experiments in the absence of either CND or FMN gave no significant product formation whereas the whole system produced enantiomerically pure (*R*)-1-phenyl ethanol (98 % ee) (Figure 8 c). Compared to the previously used Au-TiO<sub>2</sub> the overall reaction rates were significantly higher as compared by the initial rates of 0.16 mM h<sup>-1</sup> and 0.81 mM h<sup>-1</sup> for Au-TiO<sub>2</sub> and CND, respectively. Hence, already under non-optimised conditions, almost 100000 turnovers for rAaeUPO and more than 100 for FMN were estimated. Similar results were achieved under the same

conditions for the hydroxylation of cyclohexane (Supplementary Figure 37). It is also worth noting that the overoxidation rate was reduced significantly.

Overall, we have combined photochemical water oxidation-catalysis with peroxygenase-catalysis to achieve visible light-driven, aerobic oxidation of hydrocarbons. Combined with further (enzymatic) reaction steps this method gives access to a broad range of functionalised building blocks starting from simple alkanes. Admittedly, the system reported here falls short in terms of space-time-yields to be economical or environmentally benign. Particularly the low concentrations of the hydrophobic substrates need to be increased and mass balance issues of some volatile reagents will have to be addressed. But the catalytic turnover achieved for the biocatalyst compares well with the state-of-the-art in peroxygenase reactions and surpasses the performance of the established P450 monooxygenases and chemical catalysts (Supplementary Table 5). Further improvements may be expected in the near future from optimised reaction schemes, particularly from more active WOCs.

## Methods

### Materials

Titanium (IV) oxide and water- $^{18}\text{O}$  (97 atom %  $^{18}\text{O}$ ) were brought from Sigma-Aldrich (The Netherlands) and used as received. Gold(III) chloride (64.4% minimum) was brought from Alfa-Aesar. All other chemicals were purchased commercially and used without further treatments.

### Photocatalyst preparation

Both anatase and rutile Au-TiO<sub>2</sub> catalysts were prepared by deposition-precipitation method according to literature procedures.<sup>51</sup> A detailed description of the syntheses is given in the Supplementary Materials. Exemplary XRD data and TEM images of Au-TiO<sub>2</sub> are shown in Supplementary Table 1 and Supplementary Figures 1-4.

### Enzyme preparation

Recombinant expression and purification of the evolved unspecific peroxygenase mutant from *Agrocybe aegerita* (*rAaeUPO*) in *Pichia pastoris* was performed following a literature procedure.<sup>20</sup> The chloroperoxidase from *Curvularia inaequalis* (*CVCPO*) was recombinantly expressed in *Escherichia coli* following a protocol published previously.<sup>42</sup> A detailed description of the production and purification of the enzymes is given in the Supplementary Materials.

### Typical protocol for the photoenzymatic hydroxylation of alkanes

To a transparent glass vial, 5.0 mg of photocatalyst was added and suspended in 900  $\mu\text{L}$  of NaPi buffer under sonication for 5 min in an ultrasonication bath. From a stock solution, 350 nM of *rAaeAPO* and 15 mM of ethyl benzene (final concentrations) were then added and the volume of the above suspension was adjusted to 1.0 mL using NaPi buffer. The reaction vial was irradiated by visible light at 30 °C under gentle stirring in a homemade setup (see Supplementary Figure 8) equipped with white light bulb (Philips 7748XHP 150 W, see Supplementary Figure 9). The distance between the reaction vial and bulb is 3.6 cm. At

intervals, aliquots were withdrawn, extracted with ethyl acetate, dried over MgSO<sub>4</sub> and analysed by (chiral) GC. Details of gas chromatograph and temperature profiles are shown in Supplementary Table 4 and Supplementary Figures 19-27.

For detailed experimental procedures of chemoenzymatic halogenation of phenols and the multi-enzyme cascade reactions, see Supplementary Methods.

## Supplementary Material

Refer to Web version on PubMed Central for supplementary material.

## Acknowledgements

Financial support by the European Research Council (ERC Consolidator Grant No. 648026) is gratefully acknowledged. The authors thank Ben Norder for XRD, Dr. Wiel H. Evers for TEM and Prof. Fred Hagen for EPR measurements. The authors also thank Dr. Sandy Schmidt for the preparation of benzaldehyde lyase, Dr. Milja Pesic for the preparation of YqjM and Dr. Tanja Knaus for the preparation of ω-transaminases. F.G.M. received funding as a European Research Council (ERC) Starting Grant Fellow (grant agreement 638271).

## References

1. Kille S, Zilly FE, Acevedo JP, Reetz MT. Regio- and stereoselectivity of P450-catalysed hydroxylation of steroids controlled by laboratory evolution. *Nature Chem.* 2011; 3:738–743. [PubMed: 21860465]
2. Kudrik EV, Afanasiev P, Alvarez LX, Dubourdeaux P, Clemancey M, Latour JM, et al. An N-bridged high-valent diiron-oxo species on a porphyrin platform that can oxidize methane. *Nature Chem.* 2012; 4:1024–1029. [PubMed: 23174983]
3. Kamata K, Yonehara K, Nakagawa Y, Uehara K, Mizuno N. Efficient stereo- and regioselective hydroxylation of alkanes catalysed by a bulky polyoxometalate. *Nature Chem.* 2010; 2:478–483. [PubMed: 20489717]
4. Wang Y, Lan D, Durrani R, Hollmann F. Peroxygenases en route to becoming dream catalysts. What are the opportunities and challenges? *Curr Opin Chem Biol.* 2017; 37:1–9. [PubMed: 27992798]
5. Ullrich R, Nüske J, Scheibner K, Spantzel J, Hofrichter M. Novel haloperoxidase from the agaric basidiomycete *Agrocybe aegerita* oxidizes aryl alcohols and aldehydes. *Appl Environ Microbiol.* 2004; 70:4575–4581. [PubMed: 15294788]
6. Grobe G, Ullrich R, Pecyna MJ, Kapturska D, Friedrich S, Hofrichter M, et al. High-yield production of aromatic peroxxygenase by the agaric fungus *Marasmius rotula*. *AMB Express.* 2011; 1:31. [PubMed: 21988939]
7. Babot ED, del Río JC, Kalum L, Martínez AT, Gutiérrez A. Oxyfunctionalization of aliphatic compounds by a recombinant peroxxygenase from *Coprinopsis cinerea*. *Biotechnol Bioeng.* 2013; 110:2323–2332. [PubMed: 23519689]
8. van Rantwijk F, Sheldon RA. Selective oxygen transfer catalysed by heme peroxidases: synthetic and mechanistic aspects. *Curr Opin Biotechnol.* 2000; 11:554–564. [PubMed: 11102789]
9. Piontek K, Strittmatter E, Ullrich R, Gröbe G, Pecyna MJ, Kluge M, et al. Structural basis of substrate conversion in a new aromatic peroxxygenase: P450 functionality with benefits. *J Biol Chem.* 2013; 288:34767–34776. [PubMed: 24126915]
10. Molina-Espeja P, Garcia-Ruiz E, Gonzalez-Perez D, Ullrich R, Hofrichter M, Alcalde M. Directed Evolution of Unspecific Peroxxygenase from *Agrocybe aegerita*. *Appl Environ Microbiol.* 2014; 80:3496–3507. [PubMed: 24682297]
11. Bornscheuer UT, Huisman GW, Kazlauskas RJ, Lutz S, Moore JC, Robins K. Engineering the third wave of biocatalysis. *Nature.* 2012; 485:185–194. [PubMed: 22575958]

12. Roiban GD, Agudo R, Reetz MT. Cytochrome P450 catalyzed oxidative hydroxylation of achiral organic compounds with simultaneous creation of two chirality centers in a single C-H activation step. *Angew Chem Int Ed.* 2014; 53:8659–8663.
13. Joo H, Lin ZL, Arnold FH. Laboratory evolution of peroxide-mediated cytochrome P450 hydroxylation. *Nature.* 1999; 399:670–673. [PubMed: 10385118]
14. Holtmann D, Hollmann F. The Oxygen Dilemma: A Severe Challenge for the Application of Monooxygenases? *ChemBioChem.* 2016; 17:1391–1398. [PubMed: 27194219]
15. Trost BM. The atom economy - A search for synthetic efficiency. *Science.* 1991; 254:1471–1477. [PubMed: 1962206]
16. Ni Y, Fernández-Fueyo E, Baraibar AG, Ullrich R, Hofrichter M, Yanase H, et al. Peroxygenase-catalyzed oxyfunctionalization reactions promoted by the complete oxidation of methanol. *Angew Chem Int Ed.* 2016; 55:798–801.
17. Krieg T, Huttmann S, Mangold K-M, Schrader J, Holtmann D. Gas diffusion electrode as novel reaction system for an electro-enzymatic process with chloroperoxidase. *Green Chem.* 2011; 13:2686–2689.
18. Kofuji Y, Ohkita S, Shiraishi Y, Sakamoto H, Tanaka S, Ichikawa S, et al. Graphitic carbon nitride doped with biphenyl diimide: efficient photocatalyst for hydrogen peroxide production from water and molecular oxygen by sunlight. *ACS Catal.* 2016; 6:7021–7029.
19. Hirakawa H, Shiota S, Shiraishi Y, Sakamoto H, Ichikawa S, Hirai T. Au nanoparticles supported on BiVO<sub>4</sub>: effective inorganic photocatalysts for H<sub>2</sub>O<sub>2</sub> production from water and O<sub>2</sub> under visible light. *ACS Catal.* 2016; 6:4976–4982.
20. Molina-Espeja P, Ma S, Mate DM, Ludwig R, Alcalde M. Tandem-yeast expression system for engineering and producing unspecific peroxygenase. *Enz Microb Technol.* 2015; 73–74:29–33.
21. Mifsud M, Gargiulo S, Iborra S, Arends IWCE, Hollmann F, Corma A. Photobiocatalytic chemistry of oxidoreductases using water as the electron donor. *Nat Commun.* 2014; 5
22. Churakova E, Kluge M, Ullrich R, Arends IWCE, Hofrichter M, Hollmann F. Specific photobiocatalytic oxyfunctionalization reactions. *Angew Chem Int Ed.* 2011; 50:10716–10719.
23. Diesen V, Jonsson M. Formation of H<sub>2</sub>O<sub>2</sub> in TiO<sub>2</sub> photocatalysis of oxygenated and deoxygenated aqueous systems: a probe for photocatalytically produced hydroxyl radicals. *J Phys Chem C.* 2014; 118:10083–10087.
24. Teranishi M, Hoshino R, Naya S-I, Tada H. Gold-nanoparticle-loaded carbonate-modified Titanium(IV) oxide surface: visible-light-driven formation of hydrogen peroxide from oxygen. *Angew Chem Int Ed.* 2016; 55(41):12773–12777.
25. Li XZ, Chen CC, Zhao JC. Mechanism of photodecomposition of H<sub>2</sub>O<sub>2</sub> on TiO<sub>2</sub> surfaces under visible light irradiation. *Langmuir.* 2001; 17:4118–4122.
26. Dvoranová D, Barbieriková Z, Brezová V. Radical intermediates in photoinduced reactions on TiO<sub>2</sub> (an EPR spin trapping study). *Molecules.* 2014; 19:17279. [PubMed: 25353381]
27. Schneider J, Matsuoka M, Takeuchi M, Zhang J, Horiuchi Y, Anpo M, et al. Understanding TiO<sub>2</sub> photocatalysis: mechanisms and materials. *Chem Rev.* 2014; 114:9919–9986. [PubMed: 25234429]
28. Marquez LA, Dunford HB. Reaction of compound III of myeloperoxidase with ascorbic acid. *J Biol Chem.* 1990; 265:6074–6078. [PubMed: 2156842]
29. Bilski P, Reszka K, Bilaska M, Chignell CF. Oxidation of the spin trap 5,5-Dimethyl-1-pyrroline N-oxide by singlet oxygen in aqueous solution. *J Am Chem Soc.* 1996; 118:1330–1338.
30. Hanaor DAH, Sorrell CC. Review of the anatase to rutile phase transformation. *J Mat Sci.* 2011; 46:855–874.
31. Fitzpatrick TB, Amrhein N, Macheroux P. Characterization of YqjM, an old yellow enzyme homolog from *Bacillus subtilis* involved in the oxidative stress response. *J Biol Chem.* 2003; 278:19891–19897. [PubMed: 12660247]
32. Hanefeld U, Gardossi L, Magner E. Understanding enzyme immobilisation. *Chem Soc Rev.* 2009; 38:453–468. [PubMed: 19169460]
33. Guo Q, Yue Q, Zhao J, Wang L, Wang H, Wei X, et al. How far can hydroxyl radicals travel? An electrochemical study based on a DNA mediated electron transfer process. *Chem Commun.* 2011; 47:11906–11908.

34. Peter S, Karich A, Ullrich R, Grobe G, Scheibner K, Hofrichter M. Enzymatic one-pot conversion of cyclohexane into cyclohexanone: Comparison of four fungal peroxygenases. *J Mol Catal B Enzym.* 2014; 103:47–51.
35. Kluge M, Ullrich R, Scheibner K, Hofrichter M. Stereoselective benzylic hydroxylation of alkylbenzenes and epoxidation of styrene derivatives catalyzed by the peroxygenase of *Agroclybe aegerita*. *Green Chem.* 2012; 14:440–446.
36. Peter S, Kinne M, Wang XS, Ullrich R, Kayser G, Groves JT, et al. Selective hydroxylation of alkanes by an extracellular fungal peroxygenase. *FEBS J.* 2011; 278:3667–3675. [PubMed: 21812933]
37. Sehl T, Hailes HC, Ward JM, Wardenga R, von Lieres E, Offermann H, et al. Two steps in one pot: enzyme cascade for the synthesis of nor(pseudo)ephedrine from inexpensive starting materials. *Angew Chem Int Ed.* 2013; 52:6772–6775.
38. Hailes HC, Rother D, Muller M, Westphal R, Ward JM, Pleiss J, et al. Engineering stereoselectivity of ThDP-dependent enzymes. *FEBS J.* 2013; 280:6374–6394. [PubMed: 24034356]
39. Höhne M, Schätzle S, Jochens H, Robins K, Bornscheuer UT. Rational assignment of key motifs for function guides in silico enzyme identification. *Nat Chem Biol.* 2010; 6:807–813. [PubMed: 20871599]
40. Hanson RL, Davis BL, Chen YJ, Goldberg SL, Parker WL, Tully TP, et al. Preparation of (*R*)-amines from racemic amines with an (*S*)-amine transaminase from *Bacillus megaterium*. *Adv Synth Catal.* 2008; 350:1367–1375.
41. Both P, Busch H, Kelly PP, Mutti FG, Turner NJ, Flitsch SL. Whole-cell biocatalysts for stereoselective C–H amination reactions. *Angew Chem Int Ed.* 2016; 55:1511–1513.
42. Fernández-Fueyo E, van Wingerden M, Renirie R, Wever R, Ni Y, Holtmann D, et al. Chemoenzymatic halogenation of phenols by using the haloperoxidase from *Curvularia inaequalis*. *ChemCatChem.* 2015; 7:4035–4038.
43. van Schijndel J, Vollenbroek E, Wever R. The chloroperoxidase from the fungus *Curvularia inaequalis* - a novel vanadium enzyme. *Biochim Biophys Acta.* 1993; 1161:249–256. [PubMed: 8381670]
44. Frank A, Seel CJ, Groll M, Gulder T. Characterization of a cyanobacterial haloperoxidase and evaluation of its biocatalytic halogenation potential. *ChemBioChem.* 2016; 17:2028–2032. [PubMed: 27542168]
45. Getrey L, Krieg T, Hollmann F, Schrader J, Holtmann D. Enzymatic halogenation of the phenolic monoterpenes thymol and carvacrol with chloroperoxidase. *Green Chem.* 2014; 16:1104–1108.
46. Martin DJ, Qiu K, Shevlin SA, Handoko AD, Chen X, Guo Z, et al. Highly efficient photocatalytic H<sub>2</sub> evolution from water using visible light and structure-controlled graphitic carbon nitride. *Angew Chem Int Ed.* 2014; 53:9240–9245.
47. Zhang W, Bariotaki A, Smonou I, Hollmann F. Visible-light-driven photooxidation of alcohols using surface-doped graphitic carbon nitride. *Green Chem.* 2017; 19:2096–2100.
48. Liu J, Zhao S, Li C, Yang M, Yang Y, Liu Y, et al. Carbon nanodot surface modifications initiate highly efficient, stable catalysts for both oxygen evolution and reduction reactions. *Adv Energ Mat.* 2016; 6:1502039–1502039.
49. Martindale BCM, Hutton GAM, Caputo CA, Reisner E. Solar hydrogen production using carbon quantum dots and a molecular Nickel catalyst. *J Am Chem Soc.* 2015; 137:6018–6025. [PubMed: 25864839]
50. Hutton GAM, Reuillard B, Martindale BCM, Caputo CA, Lockwood CWJ, Butt JN, et al. Carbon dots as versatile photosensitizers for solar-driven catalysis with redox enzymes. *J Am Chem Soc.* 2016; 138:16722–16730. [PubMed: 27977174]
51. Priebe JB, Radnik J, Lennox AJJ, Pohl MM, Karnahl M, Hollmann D, et al. Solar hydrogen production by plasmonic Au-TiO<sub>2</sub> catalysts: impact of synthesis protocol and TiO<sub>2</sub> phase on charge transfer efficiency and H<sub>2</sub> evolution rates. *ACS Catal.* 2015; 5:2137–2148.

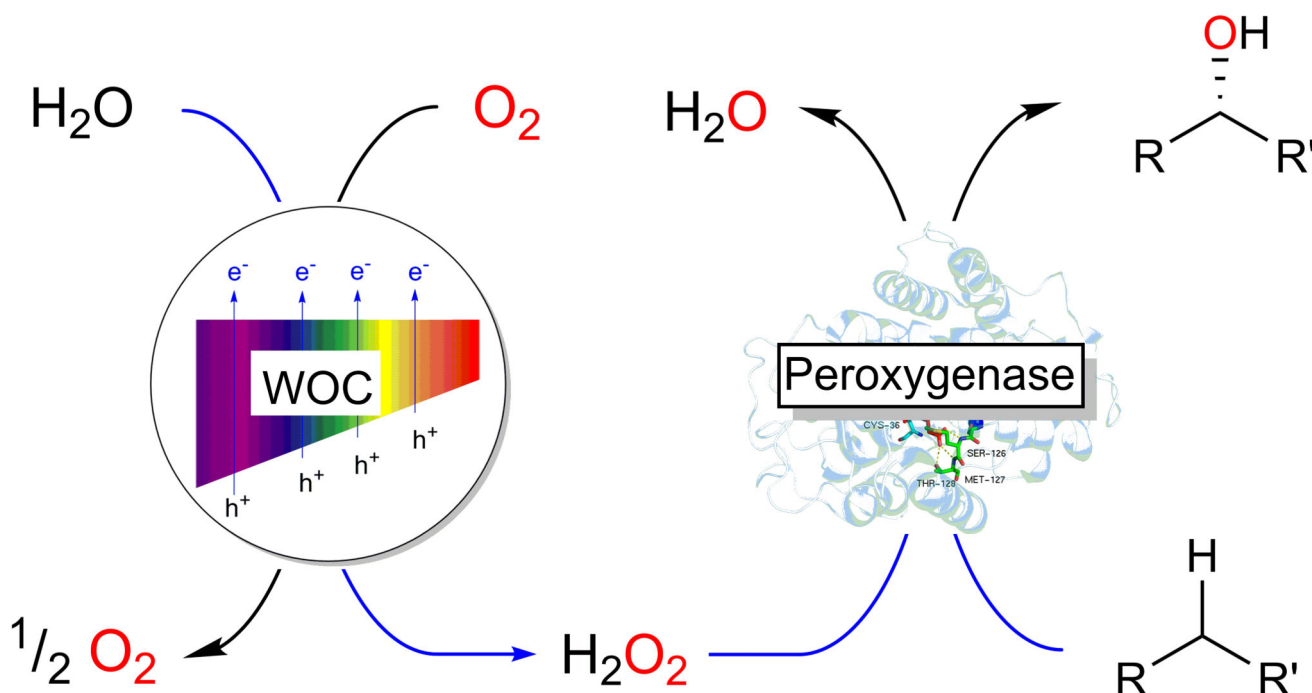


**Figure 1. Photochemical water oxidation generating  $\text{H}_2\text{O}_2$  to promote peroxygenase-catalysed hydroxylations.**

A water oxidation catalyst (WOC) mediates the photochemical oxidation of water and delivers the reducing equivalents liberated to molecular oxygen to produce  $\text{H}_2\text{O}_2$ . The latter is utilised by a peroxygenase to catalyse (stereo)selective oxyfunctionalisation reactions.

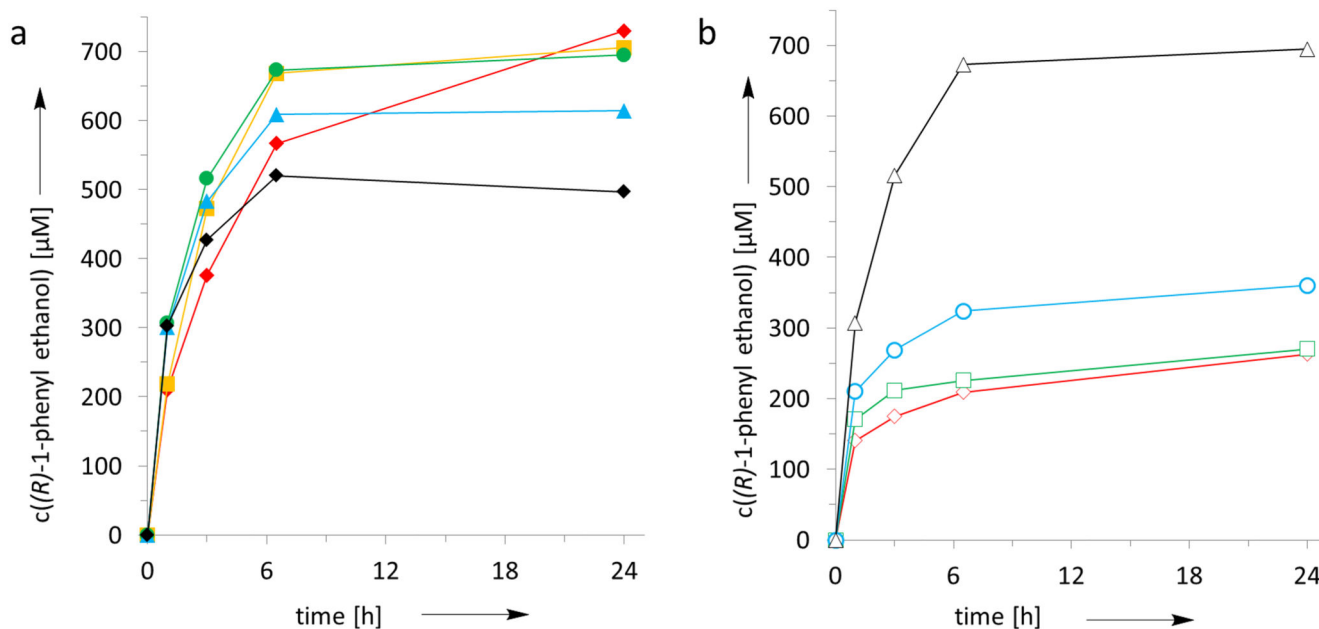
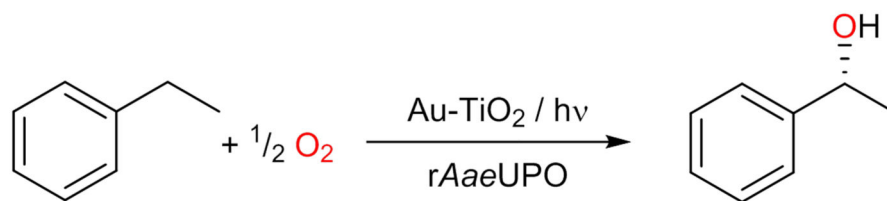


**Figure 2.** Time courses of the photoenzymatic hydroxylation of ethyl benzene at varying catalyst concentrations.

General conditions: reactions were performed in 60 mM phosphate buffer (pH 7.0) under visible light illumination ( $\lambda > 400$  nm),  $T = 30$  °C,  $c(\text{ethyl benzene}) = 15$  mM. A:  $c(\text{rAaeUPO}) = 350$  nM,  $c(\text{Au-TiO}_2) = 1$  gL<sup>-1</sup> (◆), 2.5 gL<sup>-1</sup> (■), 5 gL<sup>-1</sup> (●), 10 gL<sup>-1</sup> (▲), 15 gL<sup>-1</sup> (◆); B:  $c(\text{Au-TiO}_2) = 5$  gL<sup>-1</sup>,  $c(\text{rAaeUPO}) = 10$  nM (◇), 50 nM (□), 150 nM (○), 300 nM (△).

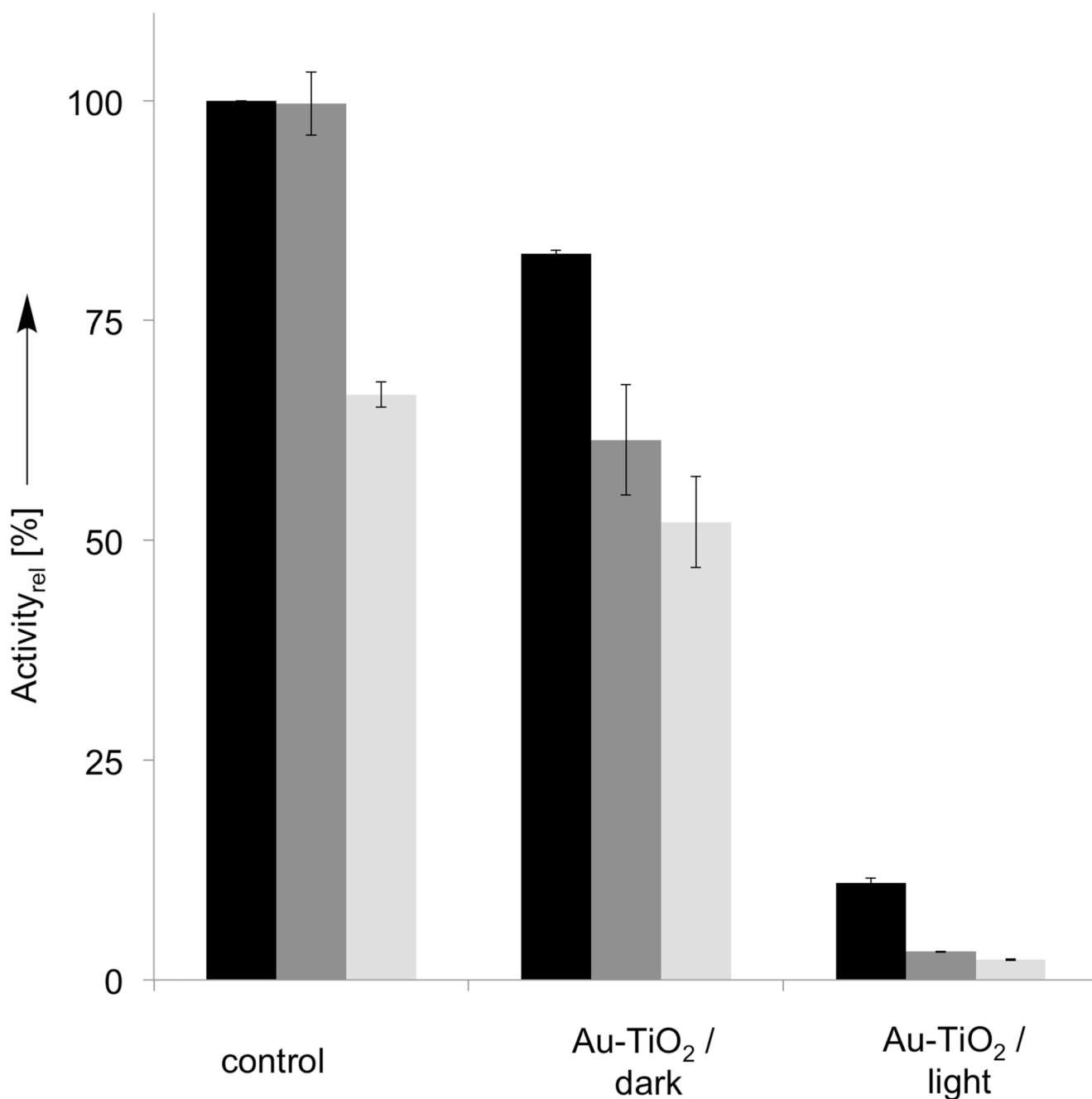


**Figure 3. Stability of rAaeUPO in the presence of anatase-Au-TiO<sub>2</sub>.**

General conditions: phosphate buffer (60 mM, pH 7.0), T= 30 °C, c(anatase Au-TiO<sub>2</sub>) = 0 (control, under illumination) or 10 gL<sup>-1</sup>, c(rAaeUPO) = 150 nM. The samples were either kept in the darkness or illuminated under visible light illumination ( $\lambda > 400$  nm). At intervals (1h (black), 5h (dark grey) and 24 h (light grey)) samples were withdrawn from the incubation mixtures and analysed for peroxygenase activity. Error bars indicate the standard deviation of duplicate experiments (n=2).

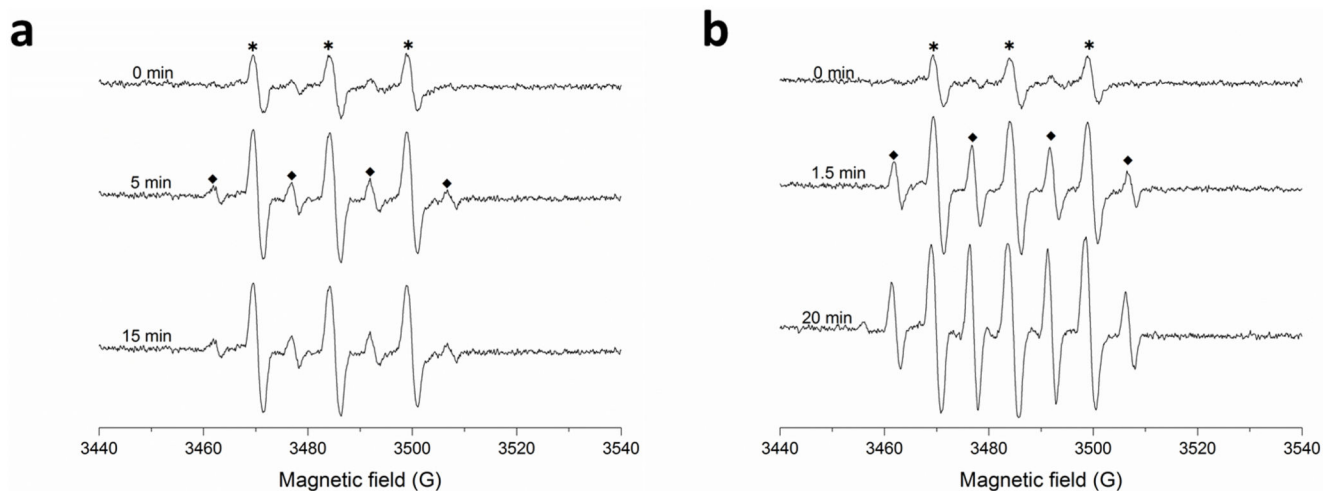


**Figure 4. EPR spectra recorded during the illumination of anatase (a) and rutile (b) Au-TiO<sub>2</sub> in water.**

Signals marked with asterisk belong to the existing oxidation product of DMPO, 5,5-dimethyl-2-oxopyrroline-1-oxyl (DMPOX); signals marked with solid diamonds belong to the spin-adduct  $\bullet$ DMPO-OH, which is not overlapping the signals of DMPOX and therefore provides sufficient quality for analysis. Reaction condition: Au-TiO<sub>2</sub> = 5.0 mg mL<sup>-1</sup>, c(DMPO) = 30 mM, RT,  $h\nu > 400$  nm. DMPO = 5,5-Dimethyl-1-pyrroline *N*-oxide.

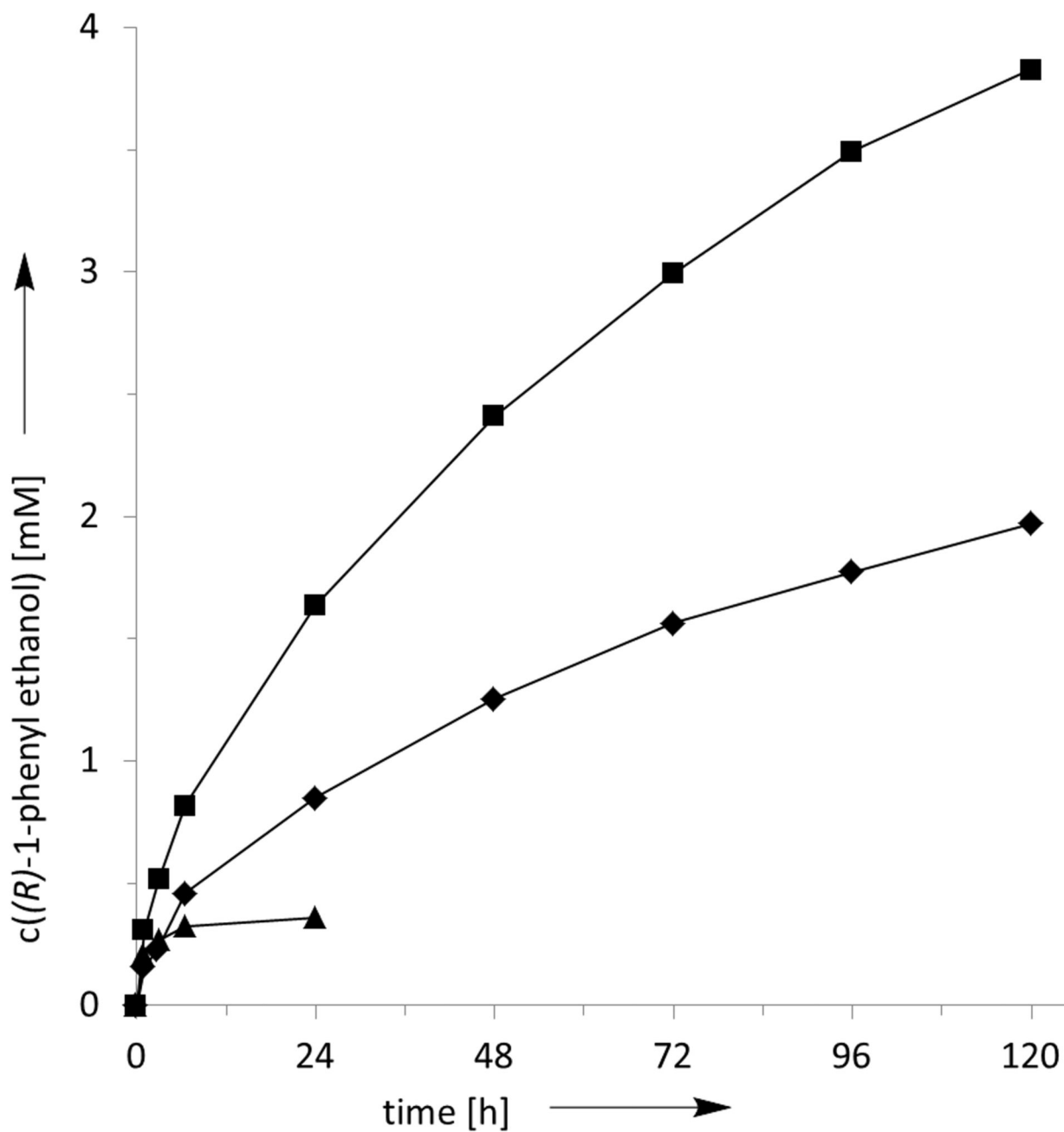


**Figure 5. Effect of reducing the interaction of rAaeUPO with the TiO<sub>2</sub> surface on the robustness of the photoenzymatic reaction.**

(▲): original reaction setup with dissolved rAaeUPO and anatase-Au-TiO<sub>2</sub>, (◆) reaction using immobilised rAaeUPO and anatase-Au-TiO<sub>2</sub>, (■): dissolved rAaeUPO with hydrophobic rutile-Au-TiO<sub>2</sub>. General conditions:  $c(\text{rAaeUPO}) = 150 \text{ nM}$  (dissolved)  $120 \text{ nM}$  (immobilised),  $c(\text{Au-TiO}_2) = 5 \text{ g L}^{-1}$ ,  $c(\text{ethyl benzene})_0 = 15 \text{ mM}$  ethyl benzene in  $60 \text{ mM}$  phosphate buffer (pH 7.0) under visible light illumination ( $\lambda > 400 \text{ nm}$ ).

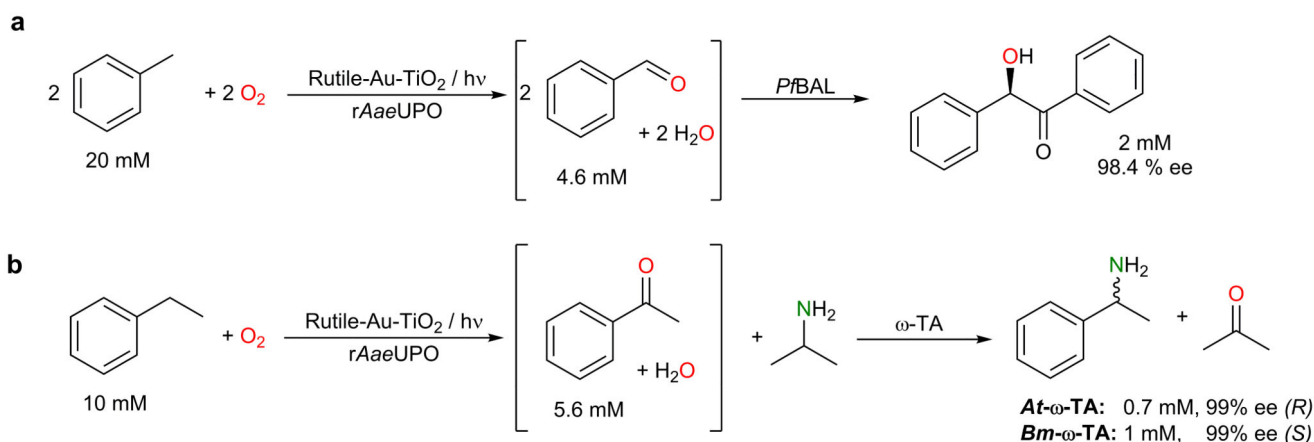


**Figure 6. Photoenzymatic cascade reactions.**

A: for the transformation of toluene to (*R*)-benzoin and b: for the transformation of ethyl benzene to (*R*)- or (*S*)-1-phenyl ethyl amine. Conditions: a): c(toluene) = 20.0 mM, c(rutile Au-TiO<sub>2</sub>) = 30 g L<sup>-1</sup>, c(rAaeUPO) = 150 nM in phosphate buffer (pH 7.0, 60 mM), T = 30 °C, 96 h, visible light illumination ( $\lambda > 400$  nm). In the second step, 100  $\mu$ L of mixture in phosphate buffer (500 mM, pH 8.5) containing 5 mM of thiaminpyrophosphate (TPP), 25 mM of MgCl<sub>2</sub> and 10 mg of crude cell extract containing *P/BAL* were added. B): c(ethyl benzene) = 10.0 mM, c(rutile Au-TiO<sub>2</sub>) = 30 g L<sup>-1</sup>, c(rAaeUPO) = 150 nM in phosphate buffer (pH 7.0, 60 mM), T = 30 °C, 96 h. In the second step, 105  $\mu$ L of isopropylamine, 130  $\mu$ L of phosphoric acid (5 M), 100  $\mu$ L of pyridoxal phosphate (PLP, 10 mM) and 10 mg of crude cell extract containing  $\omega$ -transaminase were added. The pH of above mixture was adjusted to approx. 9.0. The dilution factor of the reaction system was 1.0/1.335 = 0.75. After the first steps under illumination and initiation of the second steps the resulting reaction mixture of both cascades was shaken at 30 °C for 40 h in the darkness

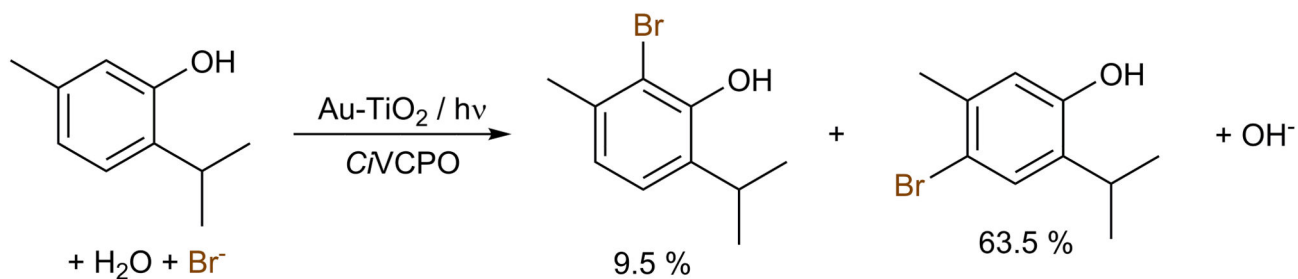


**Figure 7. Photoenzymatic halogenation of thymol.**

Conditions:  $c(\text{rutile Au-TiO}_2) = 5 \text{ gL}^{-1}$ ,  $c(\text{CVCPO}) = 150 \text{ nM}$ ,  $c(\text{thymol}) = 3 \text{ mM}$ ,  $c(\text{KBr}) = 6 \text{ mM}$ ,  $c(\text{Na}_3\text{VO}_4) = 50 \text{ }\mu\text{M}$  in 1.0 mL citrate buffer (50 mM, pH 5.0)  $T = 30 \text{ }^\circ\text{C}$ ,  $t = 70 \text{ h}$ . The reaction mixture was irradiated by visible light ( $\lambda > 400 \text{ nm}$ ).

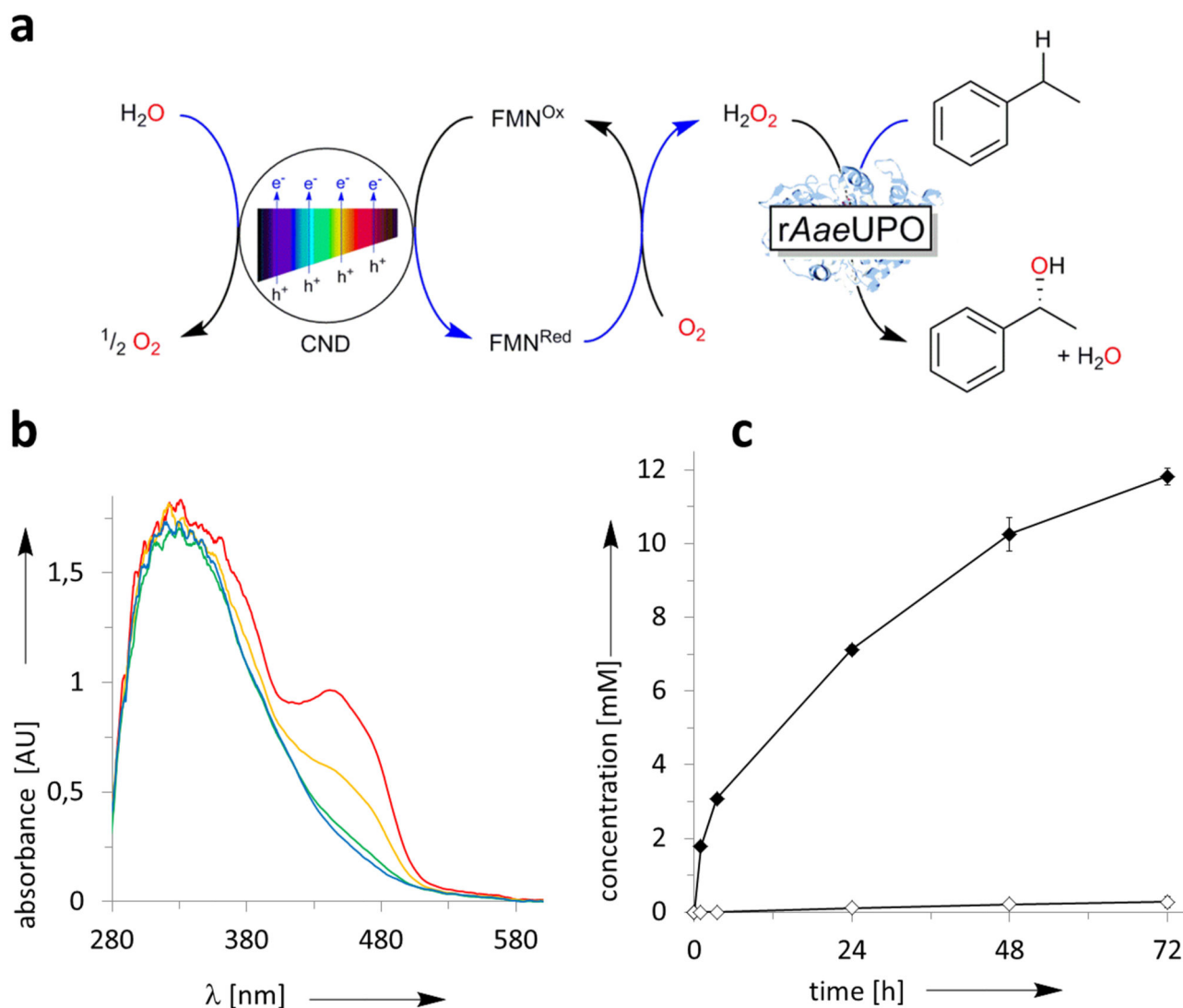


**Figure 8. Photoenzymatic reactions using carbon-nano-dot photocatalysts and FMN-cocatalysts.** a: Proposed reaction scheme; b: UV-spectroscopic investigation of the photocatalytic reduction of FMN and c: exemplary time course of the complete reaction system. General conditions: b: The reaction was performed under anaerobic conditions in a glove box. Reaction condition:  $[CND] = 1 \text{ g L}^{-1}$  and  $[FMN] = 0.05 \text{ mM}$  in phosphate buffer pH 7.0 (60 mM),  $\lambda = 450 \text{ nm}$ , at intervals (0 (red), 5 (orange), 15 (green) and 30 (blue) min) the reaction mixtures were analysed by UV/Vis spectroscopy; c:  $[rAaeUPO] = 120 \text{ nM}$ ,  $[\text{ethyl benzene}] = 15 \text{ mM}$ ,  $[CD] = 5 \text{ g L}^{-1}$  and  $[FMN] = 0.1 \text{ mM}$  in 60 mM phosphate buffer (pH 7.0) under visible light irradiation ( $\lambda > 400 \text{ nm}$ ). Error bars indicate the standard deviation of duplicate experiments ( $n=2$ ).

Table 1

Substrate scope of the photobiocatalytic hydroxylation reaction.<sup>[a]</sup>

Entry <sup>[a]</sup>	product	mM <sup>[b]</sup>	ee [%] <sup>[b]</sup>	Other products	mM <sup>[b]</sup>	Yield, % <sup>[b]</sup>	TON, 103 <sup>[b]</sup>
1		4.1	/		0.5	45.2	30.1
2		4.2	/		0.1	43.1	28.7
3		2.6	/		0.1	26.7	17.8
4		2.3	>99		0.5	28.2	18.8
5		3.6	95.2		1.0	45.8	30.5
6		5.0	75.0		0.8	58.2	38.8
7		0.3	78.5		0.2	4.8	3.2

<sup>[a]</sup> Conditions: c(substrate)<sub>0</sub> = 10.0 mM, c(rutile Au-TiO<sub>2</sub>) = 10 g L<sup>-1</sup>, c(rAaeUPO) = 150 nM (dissolved), in phosphate buffer (pH 7.0, 60 mM), T = 30 °C, 70 h, visible light illumination (λ > 400 nm). n.d. = not determined.

<sup>[b]</sup> based on the concentration of both products.